Adsorption of Atomic H and O on the (111) Surface of Pt_3Ni Alloys

Timo Jacob and William A. Goddard, III*

Materials and Process Simulation Center, Beckman Institute (139-74), California Institute of Technology, 91125 Pasadena, California

Received: January 2, 2004; In Final Form: April 15, 2004

To determine the optimal structure and size of a cluster suitable for modeling chemical processes on the (111) surface of Pt_3Ni alloys and to understand how alloying changes the electronic structure, we used the B3LYP flavor of density functional theory (DFT) to study systematically the composition and the characteristics of the Pt/Ni(111) alloy surface for clusters up to 44 atoms. We find that the bulk structure (Pt_3Ni crystal) has the atoms cubic closest packed as in bulk Pt or bulk Ni, but ordered such that each Ni has 12 bonds to Pt atoms and we find that this same pattern is preferred on the (111) surface. As a result, the ordered (111) surface has each Ni surrounded by six Pt atoms. After determining the optimal cluster, we examined the chemisorption of atomic hydrogen and atomic oxygen at all on-top (μ_1), bridge (μ_2), and 3-fold (μ_3) sites on the (111) alloy surface. We find that oxygen binds most strongly at a fcc site (two Pt and one Ni atom) with an adsorption energy of 3.50 eV, which is 0.22 eV stronger than binding to the pure Pt(111) surface. The barrier for the O to migrate about fcc sites shared by the same Ni is 0.23 eV, but to hop over to a site bordering a different Ni is 0.53 eV. In contrast, the barrier on Pt(111) is 0.56 eV. Thus oxygen is much more localized on the Pt/Ni alloy surface than on pure Pt. A similar behavior was observed for the chemisorption of hydrogen. Here we find that the best site is on-top of Pt with $D_e = 2.67$ eV, which is comparable to pure Pt(111). In contrast to Pt(111) where the barrier for migration through the bridge and fcc sites is only 0.06 eV, making H very mobile, we find that on Pt/Ni(111) the adsorption energies range from 1.78 to 2.67 eV. Here the migration of the H from one Pt site to the next goes through the bridging and fcc sites sharing a Ni with a barrier of 0.12 eV, twice that for Pt(111).

1. Introduction

Low-temperature polymer electrolyte membrane fuel cells (PEM-FCs) are most promising toward efficient and environmentally clean sources of power for transportation. Assuming a source for H_2, the cleanest system is the H_2 fuel cell, which oxidizes H_2 at the anode to provide electrons for power and protons that migrate to the cathode to reduce O_2 with H_2O as the only product. A major impediment here is that the oxygen reduction reaction (ORR) at the cathode is too slow, limiting the performance of the PEM fuel cell.[1] Thus, during the past decade there has been an enormous effort to improve or replace the current generation of Pt and Pt-based catalysts to reduce the kinetic limitations at the cathode.[2] In particular, there has been a great deal of effort toward using Pt alloys.[3−8] Experimentally, it is observed that Pt/Ni alloys lead to enhanced reaction rates for the oxygen reduction step of the cathode reactions.[7] However, there remains considerable uncertainty about the mechanisms underlying this enhancement:

- How does the modified electronic structure of the Pt/Ni alloy differ from the pure Pt catalyst?
- What aspect of this difference between Pt and the alloy affects the rates?
- How is the reaction pathway on the alloy surface different from that on the pure Pt catalyst?

Indeed, it might not even be the catalyst itself that is different, but rather the surface structure or the way the surface interacts with the acid sites of the PEM (delivering the proton) that is different.

Experimentally, a variety of Pt/Ni alloy crystals ($Pt_{0.1}Ni_{0.9}$, $Pt_{0.25}Ni_{0.75}$, $Pt_{0.5}Ni_{0.5}$, and $Pt_{0.78}Ni_{0.22}$) have been studied using low-energy electron diffraction (LEED), X-ray photoelectron spectroscopy (XPS), and medium energy ion scattering (MEIS). A good overview is given by Vasiliev[9] and Lundberg.[10] It has been found that Pt/Ni forms fcc solid solutions over the whole range of compositions.[11] Concerning the ordering of the surface Bardi et al. have shown that the similar system $Pt_3Co(111)$ first forms an ordered fcc-like structure, which during the UHV treatment changes to a disordered structure.[12] This finally leads to segregation on the surface. For example, the $Pt_{0.78}Ni_{0.22}(111)$ surface, which is of particular interest in this paper, shows a Pt enriched surface followed by a damped oscillatory Pt/Ni composition profile in the first three surface layers.[13] Despite the segregation, the surface relaxation is less than 2%.[10]

To lay a basis for optimizing the catalytic alloy properties, it is useful to study clean well-ordered surfaces. Thus Paulus et al. applied multiple cycles of surface sputtering and annealing procedures to prepare an ordered Pt_3Ni surface, which was used to study enhancement effects on the oxygen reduction reaction.[7]

To better understand the mechanisms by which the changes in the catalyst caused by alloying the Pt system modify the rates of the reactions, we undertook a series of first principles quantum mechanics calculations to study the Pt/Ni alloy system. Performing systematic calculations on various clusters with different Ni−Pt compositions with up to 44 atoms, here we report the preferred geometry and the changes in the electronic structure due to the Ni atoms. We find that the geometric structure in the alloy is still dominated by the Pt, but that the Ni atoms significantly change the chemistry of the whole system. As a first step in characterizing these changes, we report the chemisorption of atomic oxygen and atomic hydrogen on the

10.1021/jp049971h CCC: $27.50
Published on Web 05/21/2004

Pt/Ni(111) alloy surface and compare with the results on pure Pt(111) surface.

In this paper section 2 describes the theoretical methods, section 3 describes the results on the alloy clusters, and section 4 discusses the chemisorption of H and O and compares with pure Pt. Finally, section 5 summarizes these results and outlines the next steps in understanding these interesting catalysts.

2. Theoretical Methods

We use the B3LYP flavor of Kohn−Sham density functional theory (DFT), which combines the B3 nonlocal hybrid GGA exchange-functional (generalized gradient approximation)[14,15] with the Lee−Yang−Parr local and nonlocal correlation functional.[15] The exchange functional combines exact Hartree−Fock (HF) exchange with the local exchange functional of Slater[17] and uses the Becke nonlocal gradient correction[18] with the Vosko−Wilk−Nusair exchange functional.[19]

Previous studies comparing the thermochemistry over the G2 data set with 148 atoms and molecules with accurately experimental energies[16] have shown that B3LYP leads to a mean average absolute error (MAD) of 0.13 eV, which can be compared to other hybrid methods (PBE1 with 0.21 eV, B3PW91 with 0.15 eV) and nonhybrid GGA methods (BLYP with 0.31 eV, BPW91 with 0.34 eV, PW91 with 0.77 eV, and PBE with 0.74 eV). Of course, all of these are much better than LDA (MAD = 3.94 eV) and HF (MAD = 6.47 eV). Because in this paper we study H and O adsorption on Pt/Ni alloy clusters, and compare these results with former studies of O and H adsorption on pure Pt clusters, where the B3LYP functional led to reliable results,[26] here we also used the B3LYP exchange-correlation functional for consistency. In addition, for the O adsorption on Pt clusters we showed that the difference in binding energy between B3LYP and BLYP (without exact HF exchange) is only 0.06 eV.[26]

All ab initio cluster calculations were carried out with the Jaguar programs.[20] For the platinum atoms the 60 core electrons (1s−4f) were described with the Hay and Wadt core-valence relativistic effective-core potential (ECP), which leaves 18 valence electrons (the atomic ground state is $(5s)^2(5p)^6(5d)^9(6s)^1(6p)^0$).[21] This uses angular momentum projection operators (nonlocal ECP) to enforce the Pauli principle.[22−25] In the Jaguar program this ECP uses the LACVP** basis set in which oxygen is described with all electrons using the 6-31G** basis set. Elsewhere we showed[26] that including additional diffuse functions on the adsorbate (even on the electronegative oxygen, which gains up to 0.5e) has only a minor influence on adsorption energy (≈0.015 eV) and charge transfer (≈0.02e).[26] Because the ground states of these clusters have numerous unpaired spins (≈22 for a 35 atom Pt cluster), it was essential to use unrestricted DFT (UDFT) and to systematically solve for the optimum spin state. In each case the total energy for all low-lying spin states was calculated self-consistently to obtain the correct ground spin states. For each of these spins, we examined all low-lying excitations between various occupied and empty molecular orbitals to ensure that we found the ground state.

All calculations on two-dimensional (slab) and three-dimensional (bulk) periodic systems were performed using the SeqQUEST DFT program,[27] which uses Gaussian basis sets rather than plane waves. These calculations used the PBE GGA functional by Perdew, Burke, and Ernzerhof.[28] For Pt the 5d and 6s electrons were placed in the valence space, the remaining core was treated with an pseudopotential.[29] These calculations used Gaussian contracted basis sets optimized at the "double-ζ plus polarization" level. After convergence tests a grid density of 10 pts./Å was applied. Making use of the particular symmetry the converged Brillouin zone (BZ) sampling used a *k*-grid with 56 special points in the irreducible BZ for the bulk studies and 34 *k*-points for the slab calculations.

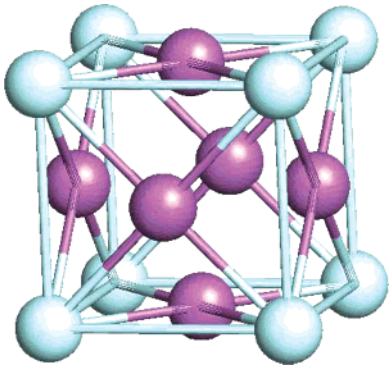

Figure 1. Model of the fcc-like Pt_3Ni bulk unit cell used to calculate the bulk lattice constant. The darker atoms are Pt; all others are Ni.

3. Results on Alloy Clusters

3.1. Cluster Composition and Model. Before determining the surface composition of the Pt/Ni alloy, we performed periodic bulk calculations (see section 2) to obtain the bulk lattice constant. Because both homologous elements Pt and Ni by themselves form fcc bulk structures, and experiments conclude that in the bulk of the alloy a 3:1 ratio is more likely,[9,12] we used a fcc-like unit cell, where all corner atoms are Ni and the rest are Pt atoms (see Figure 1). This leads to the $Pm\bar{3}m$ space group. We find an optimized lattice constant of 3.89 Å. This can be compared to our calculated lattice constants for Pt and Ni of 3.96 and 3.61 Å, respectively, leading to a weighted average of 3.87 Å (only 0.02 Å smaller than the calculated alloy value). The experimental lattice constants[30,31] are 3.92 Å (Pt) and 3.52 Å (Ni) for the pure substances. This indicates an increased bonding, perhaps due to the charge transfer or ionic character in the Ni−Pt bonds.

We calculated the cohesive energy per formula unit (four atoms) to be $E_{coh}(Pt_3Ni) = 22.63$ eV, which can be compared to the experimental values of $E_{coh}(Pt_4) = 23.36$ eV and $E_{coh}(Ni_4) = 17.76$ eV.[30] Thus, the calculated cohesive energy for the alloy is 3.1% higher than the weighted average from the pure elements. Because the lattice constant and the cohesive energy of the Pt_3Ni alloy are close to that of pure Pt, we consider that the structure and energetics of the alloy are dominated by Pt.

Using the bulk structure and calculated lattice constant of Pt_3Ni as the initial guess for the surface structure, we examined possible relaxation effects. We considered a two-dimensional periodic slab (Figure 2 shows the 2 × 2 unit cell) with a thickness of six layers. To enforce the bulk boundary conditions, the lowest three layers were fixed in their positions during the geometry optimization. Within the first layer we find an average Ni−Pt distance of 2.755 Å and Pt−Pt distance of 2.781 Å (which differs by less than 1% from the atomic distance in the bulk of 2.755 Å). Similarly, between atoms in the first and second layers, we find average distances of 2.754 Å (Ni−Pt) and 2.784 Å (Pt−Pt). This agrees with experimental observations.[13] Thus, for the cluster studies on the alloy composition, we used the calculated bulk atomic distance and fixed the atom positions.

To determine the optimal composition of Pt and Ni in the alloy system, we started with a three-atom cluster and increased the size successively up to 44 atoms. For almost every system

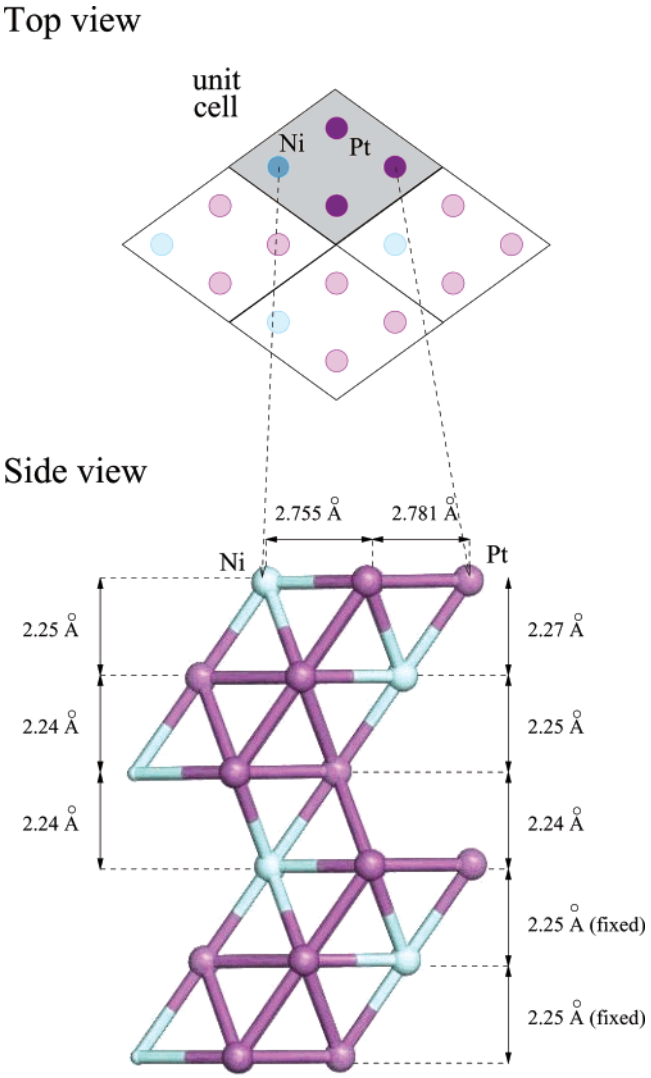

Figure 2. Model of the six-layer 2 × 2-unit cell used in periodic slab calculations to study possible relaxation effects. The upper figure is a top view on the surface and shows how the unit cell is repeated periodically. The lower figure is a side view of the unit cell after the geometry optimization of the first three surface layers. The new distances indicate that minor relaxation effects occur.

both the composition and the position of the different elements were varied. By comparing the total energies for the ground spin state of each system, we found the most stable configuration (we also checked the total energies for all low-lying spin states to obtain the correct ground spin states). For example, Figure 3 shows all six-atom clusters that were considered. We started with Pt_5Ni_1 and varied the position of the Ni atom. Two different configurations could be distinguished. Afterward, another Pt was exchanged by a Ni atom, leading to Pt_4Ni_2. The four possible clusters are shown in the second and third row of Figure 3. Finally, the composition was changed to Pt_3Ni_3, leading to the last five clusters shown in the same figure. In extensive studies the same procedure was performed for most of the following clusters (the indices denote the number of atoms per layer, e.g., $Pt_{5.2}Ni_{1.1}$ means five Pt and one Ni in the first layer, and two Pt and one Ni in the second layer):

- one layer: Ni_3, Pt_1Ni_2, Pt_2Ni_1, Pt_5Ni_1, Pt_4Ni_2, Pt_3Ni_3, Pt_7Ni_1, Pt_6Ni_2, Pt_5Ni_3, $Pt_{10}Ni_4$, $Pt_{11}Ni_3$, $Pt_{22}Ni_8$, $Pt_{32}Ni_{12}$
- two layer: $Pt_{5.3}Ni_{1.0}$, $Pt_{5.2}Ni_{1.1}$, $Pt_{7.4}Ni_{1.0}$, $Pt_{7.3}Ni_{1.1}$, $Pt_{11.6}Ni_{1.1}$, $Pt_{9.5}Ni_{3.2}$, $Pt_{11.10}Ni_{3.3}$, $Pt_{10.10}Ni_{4.3}$
- three layer: $Pt_{10.10.6}Ni_{4.3.2}$, $Pt_{11.9.7}Ni_{3.4.1}$, $Pt_{11.10.5}Ni_{3.3.3}$

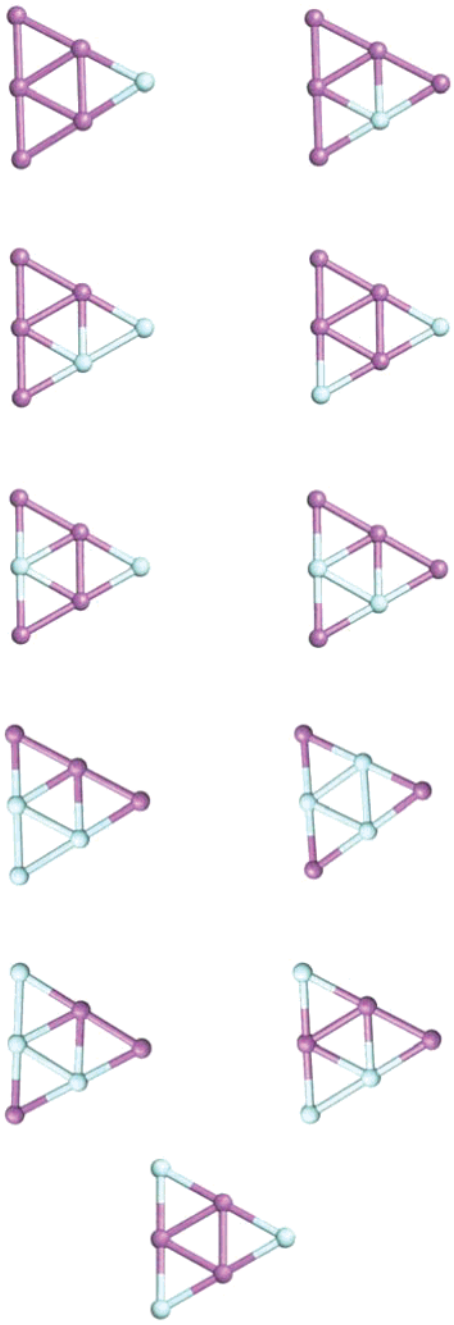

Figure 3. Models of all six atomic alloy clusters studied to find the optimal structure. The darker atoms are Pt; all others are Ni.

Because some systematics could be extracted from the smaller systems, we were able to reduce the number of larger clusters to be checked by applying these structural information. The most stable configurations for the one-layer clusters are shown in Figure 4, and Figures 5 and 6 show the most stable two- and three-layer clusters. The corresponding energetics are given in Table 1.

3.2. One-Layer Clusters. Among the three-atom clusters the Pt_2Ni has the highest net binding energy (Pt_3 excluded). Because the Pt−Pt bond is stronger than the Ni−Ni (by ≈0.9 eV) and the Pt−Ni bond (by ≈0.1 eV) this behavior was expected. However, increasing the cluster size to Pt_5Ni_1 or Pt_7Ni_1 causes significant deviations. Instead of preferring 2-fold sites (bonds to two Pt atoms), which would be consistent with a maximum number of Pt−Pt bonds, the clusters with Ni at a 4-fold site (bonds to four Pt atoms) are most stable, leading to the highest net binding energy (see Figure 4). For the single-layer clusters

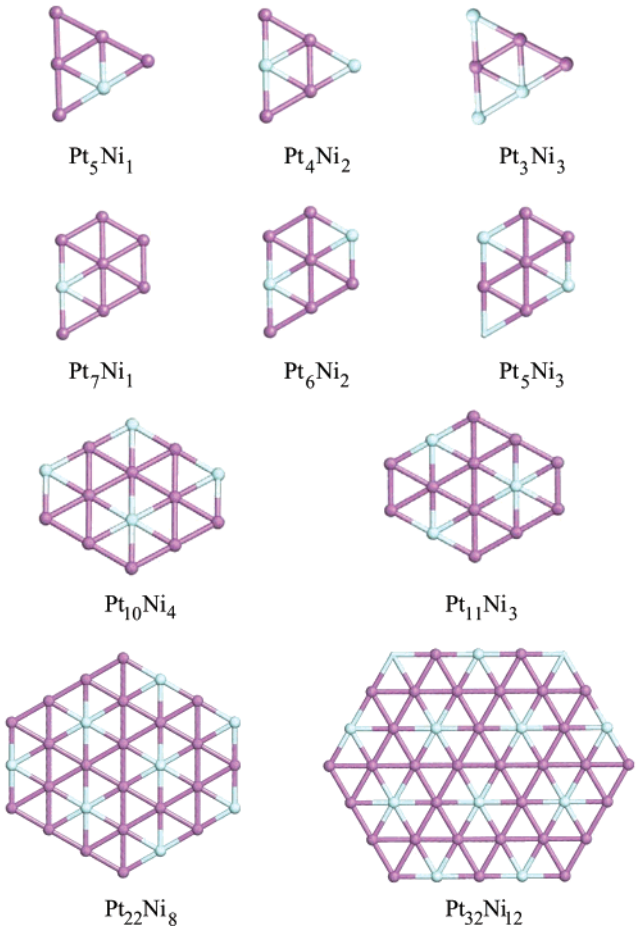

Figure 4. Optimal compositions for one-layer Pt/Ni alloy clusters. Darker atoms denote Pt; all others are Ni. The two largest clusters were only used for electronic structure purposes.

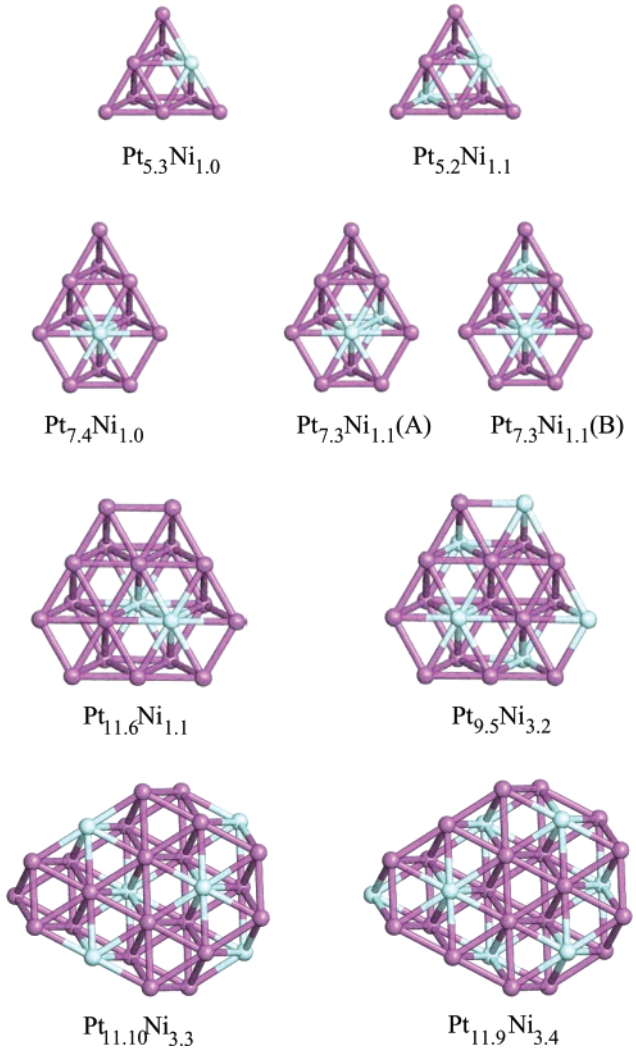

Figure 5. Optimal compositions for two-layer Pt/Ni alloy clusters. Darker atoms denote Pt; all others are Ni.

with two Ni and up to six Pt atoms we calculated the total energies of all different atom distributions. We found that adding a second Ni atom to the system does not change the preferred 4-fold site of the first atom. The position of the second Ni was found to prefer sites that are not next to the first Ni. Finally, the Pt_4Ni_2 and Pt_6Ni_2 structures shown in Figure 4 were obtained. This Pt_6Ni_2 cluster can be considered as a part of the $Pt_3Ni(111)$ surface (every Ni at the surface is surrounded by six Pt atoms, hereafter denoted as the *bulklike* structure). A similar behavior was obtained upon considering three Ni atoms. Two Ni atoms of Pt_3Ni_3 are at the same positions as before, and the third one prefers to minimize the number of Ni neighbors. This is not consistent with the bulklike structure, because this would have all three Ni as corner atoms. However, Pt_5Ni_3 again prefers the bulklike structure. It seems that the six-atom cluster is too small to carry more than one Ni.

Next we studied the two 14-atom systems consistent with the bulklike distribution: $Pt_{10}Ni_4$ and $Pt_{11}Ni_3$. On the basis of the knowledge already extracted from the smaller systems, the optimal Pt/Ni distribution was studied by displacing only the single Ni atom located at the 6-fold site (surrounded by six Pt atoms). We found the same result as obtained for the eight-atom cluster, namely, that the bulklike distribution is preferred (see Figure 4).

To understand why the single-layer system prefers a bulklike composition rather than forming a maximum amount of Pt−Pt bonds, we analyzed the distribution of charge and net spin density (obtained from the Mulliken populations). However, to minimize border effects for these studies, we used two enlarged clusters: $Pt_{22}Ni_8$ and $Pt_{32}Ni_{12}$. Because our interest was only in the net spin-density distribution, we considered only the bulklike compositions shown in Figure 4. It turned out that all inner Ni atoms have net spins between 1.1 and 1.4, essentially all of which is due to the d electrons, suggesting $d^{8.75}$ character. In addition, the Mulliken population shows a net average positive charge of 0.90e, indicating that Ni is more electropositive than Pt, as expected. This suggests an electronic configuration of $s^{0.35}d^{8.75}$. Every surrounding Pt atom has a net spin of 0.5−0.7, with an average of 0.59, essentially all of which is due to the d electrons, suggesting $d^{9.41}$. The additional average charge is −0.30e, suggesting an electronic configuration of $s^{0.89}d^{9.41}$ character. Such analysis neglects spin-pairing of singly occupied d orbitals on different centers, giving the appearance of slightly increased d character.

Similar analysis for the pure single-layer Pt clusters led to net spins of 0.83 (no net charges), suggesting an electronic configuration of $s^{0.83}d^{9.17}$ character. Thus the presence of the Ni seems to reduce the number of unpaired spins on the Pt that is important in forming covalent bonds to the adsorbate while putting more charge into the s-like character on the Pt that might favor electron transfer. This is consistent with the reduction of the bond energy of O to the pure Pt fcc site on the alloy (fcc-Pt_3), which decreases by 1.04 eV from the value on pure Pt. This analysis is consistent with the interstitial electron model

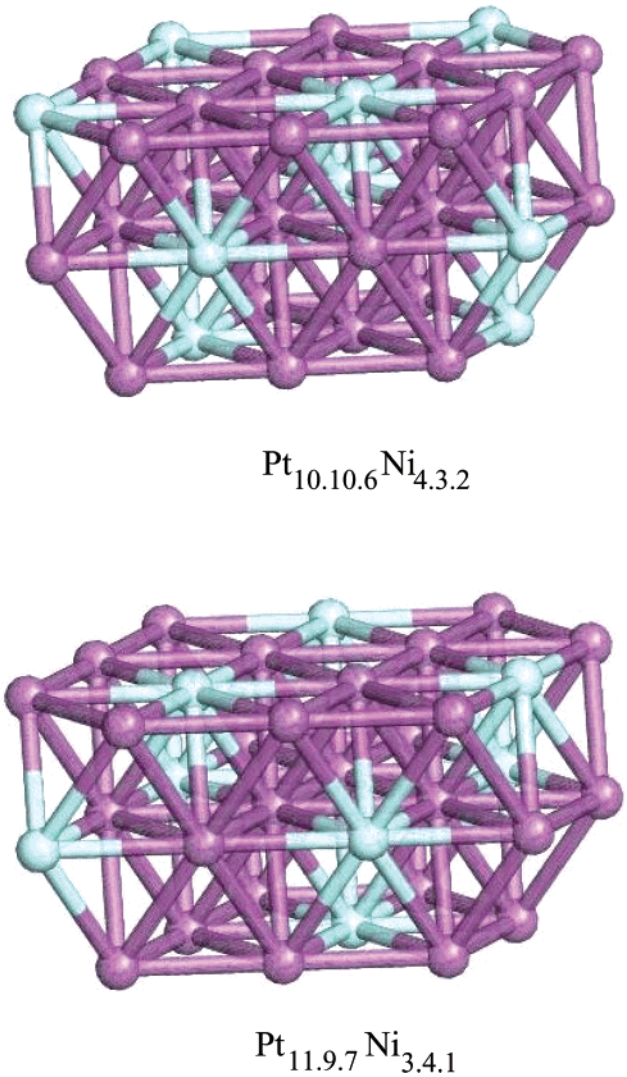

Figure 6. Models of the both three-layer Pt/Ni alloy clusters used to find the best surface representation. Darker atoms denote Pt; all others are Ni.

(IEM) and with the QM calculations on the pure Pt(111) surface, which suggest s^1d^9 character on the surface atoms.[26,32]

We also analyzed the charge distribution of less favorable structures. For example, exchanging the central Ni atom of $Pt_{11}Ni_3$ with one of the Pt atoms right of it (see Figure 4) leads to a less negative charge on Pt atoms (−0.13 to −0.22e), which have less than two Ni neighbors. Consequently, the moved Ni atom, which does not follow the bulklike structure, reduces its positive charge by 0.3−0.4e. Indeed, the perturbation of the charge distribution induced by Ni atoms, which occupy different positions than the bulklike composition, has an impact on the charges of even far atoms (secondary effect). This results in less stability and therefore higher total energies.

The preference we find for the Ni to be surrounded by Pt atoms is consistent with the energetics found for the bulk system and probably results from the ionic or electrostatic contributions to the bonding. It could also result from repulsive electrostatic interactions between the Ni atoms resulting from their net charge of 0.90e. The Pt−Ni Coulomb attraction, and the strong Ni−Ni repulsion stabilize the $Pm\bar{3}m$ (see above) structure of the bulk system, which might also help to explain the behavior of the border atoms. All Pt atoms located at the border of the cluster with a neighboring Ni atom have a net spin between 0.6 and 1.0, depending on the number of adjacent Ni atoms. Those Pt atoms with fewer neighboring Ni have higher net spins.

TABLE 1: Total Energies and Spin States for the Most Stable Compositions of Pt/Ni Alloy Clusters[a]

system	ground-state energy (hartree)	spin state	total bind. energy (eV)
Ni_3	−507.83871	2	2.700
Pt_1Ni_2	−457.71355	1	3.877
Pt_2Ni_1	−407.56714	1	4.476
Pt_5Ni_1	−765.08400	3	12.168
Pt_4Ni_2	−815.23712	3	11.751
Pt_3Ni_3	−865.37858	3	11.018
Pt_7Ni_1	−1003.43465	3	17.461
$Pt_{10}Ni_4$	−1868.96712	5	32.666
$Pt_{11}Ni_3$	−1818.81043	6	32.985
$Pt_{22}Ni_8$	−3976.48170	11	75.980
$Pt_{32}Ni_{12}$	−5845.73671	17	116.479
$Pt_{5.3}Ni_{1.0}$	−1122.70210	4	21.802
$Pt_{5.2}Ni_{1.1}$	−1172.86968	4	22.591
$Pt_{7.4}Ni_{1.0}$	−1480.25499	5	31.286
$Pt_{7.3}Ni_{1.1}$ (A)	−1530.42283	5	31.270
$Pt_{7.3}Ni_{1.1}$ (B)	−1530.42204	5	31.248
$Pt_{11.6}Ni_{1.1}$	−2364.72438	6	51.816
$Pt_{9.5}Ni_{3.2}$	−2515.21065	5	51.299
$Pt_{11.10}Ni_{3.3}$	−3518.92050	9	76.248
$Pt_{11.9}Ni_{3.4}$	−3569.13043	9	77.377
$Pt_{10.10.6}Ni_{4.3.2}$	−4623.09643	11	104.714
$Pt_{11.9.7}Ni_{3.4.1}$	−4572.96492	12	105.718

[a] Only the ground-state values are summarized. In addition, the total net binding energy of each system is listed.

3.3. Two-Layer Clusters. After finding the optimal Pt/Ni distribution for the single-layer systems we studied the influence of a second layer. Starting from clusters with six atoms in the first and three atoms in the second layer, we successively increased the cluster-size up to 14 atoms in the first and 13 in the second layer. For the smaller clusters we systematically changed both the total number of Ni atoms and the distribution in each layer. The systems found to be most stable are shown in Figure 5.

With only one Ni atom the $Pt_{5.3}Ni_{1.0}$ cluster prefers a configuration similar to that of the single-layer six-atom system. For Pt_5Ni_1 this was a 4-fold site, whereas now the corresponding site is 6-fold (four Pt neighbors in the same layer and two in the other layer). Substitution of another Pt with a Ni atom has no influence on the preferred site of the first Ni. This behavior was observed for the six-atom single-layer cluster. However, now the additional Ni atom prefers to be in the second layer rather than occupying a position in the same layer as the first Ni atom. This allows both Ni atoms to have more Pt neighbors, increasing the number of Pt−Ni bonds. The most stable structure of $Pt_{5.2}Ni_{1.1}$ is shown in Figure 5. This Pt/Ni distribution again corresponds to the $Pm\bar{3}m$ bulklike structure. A similar trend was observed for the enlarged system with eight atoms in the first and four in the second layer. Having only one Ni ($Pt_{7.4}Ni_{1.0}$) the most stable position of this atom is in the center of the first layer. Although this site is different from the eight-atom single-layer system, it again maximizes the number of Pt−Ni bonds. Just as for the smaller two-layer cluster $Pt_{5.2}Ni_{1.1}$, we find that an additional Pt atom prefers to be in the second layer. Both $Pt_{7.3}Ni_{1.1}$ configurations shown in Figure 5 have nearly the same total energy and net binding energy.

Next we studied the system with 12 atoms in the first and seven atoms in the second layer. On the basis of the results for the smaller two-layer systems, we started with two Ni in the system, where we found that the best structure $Pt_{11.6}Ni_{1.1}$ has both Ni atoms next to each other! However, this configuration also maximizes the number of Pt−Ni bonds. We added the

maximum number of Ni atoms to the 19-atom two-layer cluster consistent with every Ni in the surface prefers being surrounded by six Pt atoms. This led to $Pt_{9.5}Ni_{3.2}$ with three Ni in the first and two Ni atoms in the second layer. We tested all different positions of the two second-layer Ni and again found that the bulklike structure is most stable. The total net binding energy is comparable to $Pt_{11.6}Ni_{1.1}$ with only two Ni atoms. Thus, the reduction of the number of Pt−Pt bonds resulting from adding Ni atoms (that would reduce the total binding energy) is mostly compensated by forming the maximum number of Pt−Ni bonds.

Finally, we studied the two-layer alloy cluster with 14 atoms in the first and 13 atoms in the second layer. Because the two-layer alloy system has already been established to prefer a bulklike Pt/Ni composition, we calculated only different distributions of the Pt/Ni atoms, consistent with this structure. With seven Ni atoms the ($Pt_{11.9}Ni_{3.4}$) cluster led to a total net binding energy that is 1.13 eV higher than the system with only six Ni atoms ($Pt_{11.10}Ni_{3.3}$). We also considered the total energy of the other possible cluster with seven Ni atoms ($Pt_{10.10}Ni_{4.3}$), which we expected to be less stable because this system has three Pt−Ni bonds less. This prediction was confirmed by the calculated total binding energy, which is lower by ≈0.89 eV compared to $Pt_{11.9}Ni_{3.4}$.

For $Pt_{11.9}Ni_{3.4}$ the analysis of net spin density and charge distribution shows trends similar to the single-layer clusters. The inner Pt atoms have net spins around 0.3, whereas the border Pt have about 0.6. A similar difference of ≈0.2 was observed for $Pt_{32}Ni_{12}$. Because nearly all Ni sites of $Pt_{11.9}Ni_{3.4}$ are at the border, the net spin densities of all Ni atoms are between 1.0 and 1.3. The charge distributions also show the same trend as for the single-layer systems. Each Ni atom has a positive charge of 0.2−0.4e, and most Pt atoms are negatively charged by −0.1e. The only exceptions are the central Pt atoms that have a charge of −0.15e. These results all agree with the previously obtained results, indicating that Pt is the electron acceptor and Ni is the donor in this alloy.

3.4. Three-Layer Clusters. For the case of three-layer clusters we tested only the 35-atom system with 14 atoms in the first, 13 in the second, and eight atoms in the last layer. Keeping the bulklike Pt/Ni distribution, three different systems were considered. We found that $Pt_{11.9.7}Ni_{3.4.1}$ has the highest total binding energy (see Figure 6). Because both the first and the third layer (surfaces) have fewer Ni atoms than the second layer, which has more bulklike character, this suggests that the very top layer might have a higher Pt concentration than the bulk, concomitant with the second layer having a higher concentration of Ni than the bulk. This is consistent with the interpretations from low-energy electron diffraction (LEED), ion scattering spectroscopy, and Auger-electron spectroscopy experiments,[9,10] which indicate surface segregation of the Pt/Ni alloy. In these experiments 24% more Pt was found at the surface than expected for a homogeneous Pt_3Ni structure. On the other hand, we calculated that the $Pt_{10.10.6}Ni_{4.3.2}$ cluster, which has more Ni on the surface than in the second layer, is only 1.00 eV lower in energy. Of course, it could be that such three-layer clusters are not sufficiently large to provide reliable predictions on surface segregation because two of the three layers are surface layers. However, the result that the surface might be richer in Pt with the second layer richer in Ni is consistent with our overall concepts of bonding, namely, that Ni prefers the maximum coordination with Pt. Because $Pt_{10.10.6}Ni_{4.3.2}$ has a structure comparable to the Pt_3Ni surface used by Paulus et al.[7] this allows us to study the experimentally measured enhanced ORR rate.

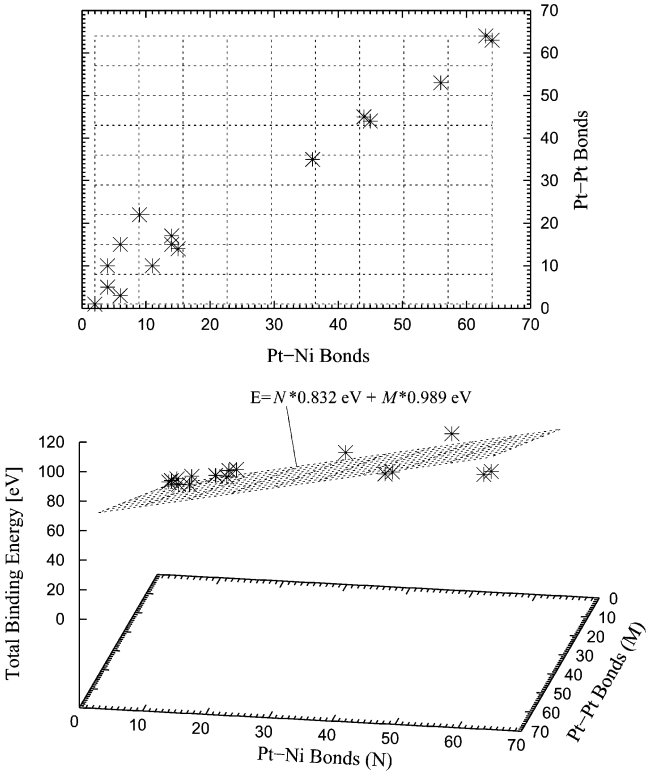

Figure 7. Total net binding energy of the most stable composition of each calculated cluster versus the number of Pt−Ni (N) and Pt−Pt (M) bonds. In addition, a plane was fitted to the values to show evidence of a linear behavior. The upper plot is a top view.

The results of the charge and net spin-density analysis of the three-layer clusters are similar to those already obtained for the one- and two-layer clusters. Thus, the surface Pt atoms have a net charge of −0.30e whereas the Ni shows a net charge of +0.90e. Because the surface ratio between Pt and Ni is 3:1, there is no net charge on the surface. Similarly, the net spin on the surface Pt atoms is 0.6 whereas the net spin on the surface Ni is 1.1. This leads to an effective hybridization at the surface of $s^{0.9}d^{9.4}$ for the Pt electronic configuration and $s^{0.2}d^{8.9}$ for the Ni. Thus, there is only a slight difference between the electronic configuration of Ni in the one-layer and three-layer clusters, which can be explained by $Pt_{11.9.7}Ni_{3.4.1}$ having the Ni sites mainly located at the border of the cluster.

3.5. Net Binding Energy. In previous work[26] we found that for pure Pt clusters there is a linear dependence between the number of Pt atoms or Pt−Pt bonds and the total net binding energy. Every additional Pt atom increased the net binding energy of the whole cluster by an average of 3.48 eV. For the alloy system such analysis is more complicated because there are two types of elements, which can each have a specific influence on the system. We chose to analyze the energetics as follows. For each Pt/Ni cluster at its most stable configuration the number of Pt−Pt and Pt−Ni bonds were counted and we searched for a possible linear relationship to the net binding energy (see Figure 7). As shown in this figure the following equation fits the calculated discrete values very well:

$$E_{\text{bind}} = N_{\text{PtNi}} \cdot 0.832\text{eV} + M_{\text{PtPt}} \cdot 0.989\text{eV}$$

where N_{PtNi} is the number of Pt−Ni bonds and M_{PtPt} is that of Pt−Pt bonds. Because the regression coefficient for this fit is $R^2 = 0.991$, we consider that the linear behavior is significant. Thus, every additional Pt−Pt bond leads to an increase of 0.989 eV in net binding energy, whereas each Pt−Ni increases it by

only 0.832 eV. As for the pure Pt clusters, where we obtained an average increase of 0.971 eV in net binding energy for every additional Pt−Pt bond ($R^2 = 0.994$), this trend seems to be more general and independent of cluster size and shape. Extrapolating these cluster results to the pure system leads to a cohesive energy (four-atom unit cell) for pure Pt of 23.30 eV, which is very close to the experimental value of 23.26 eV at 0 K.[30] For the Pt_3Ni alloy this extrapolation leads to 21.852 eV, which is 96.6% of the bulk value obtained from our calculations on the infinite crystal.

Although the energy value obtained for each Pt−Pt bond is higher than the Pt−Ni value, this result does not mean that minimizing the number of Pt−Ni bonds for a given cluster composition would create a more stable system. This expression is only correct for the optimum distribution and does not include the effect of the less unfavorable Ni−Ni bonds, which would destabilize the cluster.

4. Results for Chemisorption

Compared to a pure Pt(111) surface the Pt/Ni(111) alloy surface shows significantly different behavior for chemisorption, indicating changes in the electronic structure of the surface. To characterize these changes and the alloy surface in general, we calculated the adsorption of atomic oxygen and hydrogen at all possible surface sites. Afterward, we will compare these results with the adsorption characteristics of oxygen[26] and hydrogen[33] on the pure Pt(111) surface. There are two advantages of choosing oxygen and hydrogen as adsorbates on the surface. First, they have very different characteristics in binding to the surface. Oxygen is much more electronegative than Pt or Ni and has two unpaired electrons to bond to the Pt surface. Therefore O is expected to strongly disturb the electronic structure of the surface. Hydrogen is less electronegative than Pt but more electronegative than Ni and has only one unpaired electrons to bond to the Pt surface. Thus, these two cases probe the effects of strong and weak perturbations on the surface. Second, H and O are involved in the reduction of O_2 to H_2O, the reaction in which we are most interested.

4.1. Surface Model. To study the chemisorption on both Pt(111) and Pt/Ni(111) surfaces, we will use the finite clusters from section 3. This allows us to investigate the details of the changes in electronic structure thoroughly. In addition, these clusters should also be suitable to represent the chemistry of realistic dispersed catalysts (despite beeing not totally spherical), which have mean sizes approaching 2 nm. The disadvantage of using clusters is that we must determine the dependence of the chemistry on the cluster size (minimizing border effects). Previously, we carried out extensive studies[26] to determine the role of cluster size and cluster shape on the chemisorption of atomic oxygen on Pt(111). We found that the $Pt_{9.10.9}$ cluster is sufficient to model the Pt(111) surface, giving results similar to the infinite surface. We expect that this cluster is appropriate for chemisorption of other species because oxygen, which strongly disturbs the electronic structure of the cluster is well described. Although $Pt_{9.10.9}$ already represents the Pt(111) surface well, we used a slightly larger cluster ($Pt_{14.13.8}$) to calculate the different adsorption processes. Because it gives more (111)-like surface atoms, reducing edge effects, we chose the $Pt_{10.10.6}Ni_{4.3.2}$ system to study oxygen and hydrogen adsorptions on the alloy surface. This model accomplishes all the requirements that were determined in ref 26 and in section 3.1. It has the bulklike Pt/Ni composition, is large enough to give a suitable representation, and allows us to study all possible adsorption sites. Moreover, it conforms with the $Pt_3Ni(111)$ surface Paulus et al. used to measure the ORR rate enhancement. However, because it does not show segregation effects as experimentally measured for the undissected $Pt_3Ni(111)$ surface, $Pt_{10.10.6}Ni_{4.3.2}$ might be not suitable for these kinds of surfaces. Because a one-layer cluster was found to give good results for the adsorption of oxygen at some of the adsorption sites of pure Pt(111), we also calculated the oxygen and hydrogen adsorptions on two single-layer alloy clusters ($Pt_{10}Ni_4$ and $Pt_{11}Ni_3$).

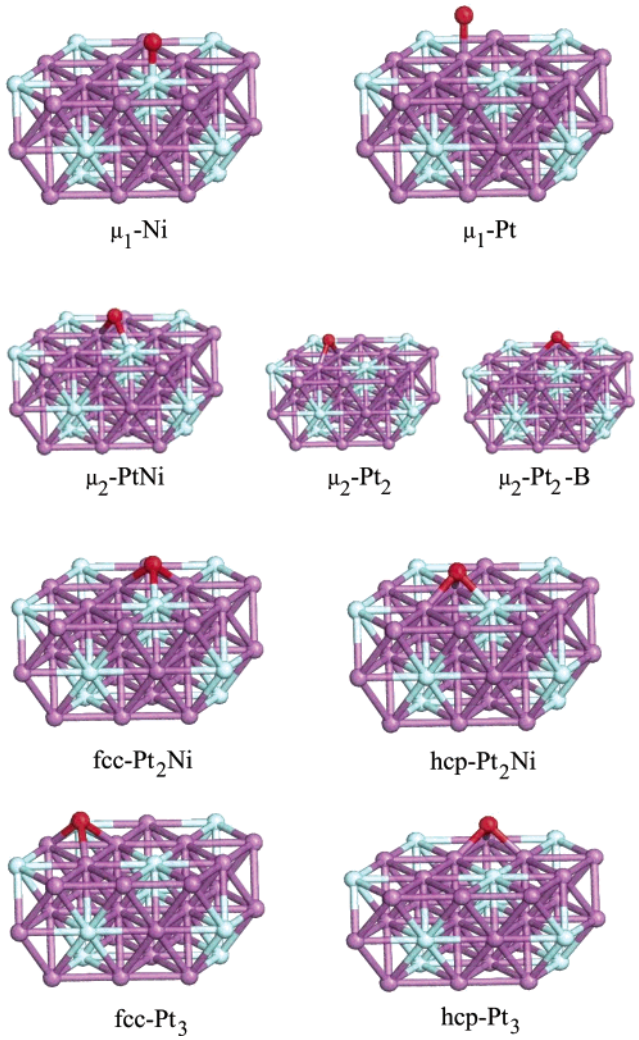

Figure 8. All adsorption sites on the Pt/Ni alloy surface (darker atoms are Pt). For pure Pt there are only four different sites (top, bridge, hcp, and fcc). The difference between μ_2-Pt_2 and μ_2-Pt_2−B is due to the different atom type of the second-layer atom located beneath the bridging site: Pt (μ_2-Pt_2) and Ni (μ_2-Pt_2−B).

Compared to the pure Pt(111) surface, which has only four different adsorption sites, the Pt/Ni(111) alloy surface is much more complex with nine different sites. All possible adsorption sites are shown in Figure 8. There exist two on-top binding sites (μ_1-Pt and μ_1-Ni), three 2-fold or bridge sites (μ_2-Pt_2, μ_2-Pt_2−B, and μ_2-PtNi), and four 3-fold sites (two fcc and two hcp, each with a μ_3-Pt_3 and a μ_3-Pt_2Ni site). The difference between μ_2-Pt_2 and μ_2-Pt_2−B comes from the type of second-layer atom located beneath the bridge site: for the first one this is another Pt atom whereas for μ_2-Pt_2−B it is Ni.

The ground spin states, adsorption energies, bond distances, and vibrational frequencies (vibration perpendicular to the surface) for the oxygen and hydrogen on the Pt/Ni(111) alloy surface are summarized in Table 3 and Table 4. For comparison we include the corresponding data on pure Pt(111) in Table 2.

TABLE 2: Ground Spin States, Adsorption Energies, and Bond Length for the Adsorption of Hydrogen on $Pt_{14.13.8}$ (S = 12 without Adsorbate), and Oxygen on $Pt_{9.10.9}$ (S = 8 without Adsorbate)[a]

system		spin state	E (eV)	R (Å)	ω (cm^{-1})
$Pt_{14.13.8}$−H	top	$^{23}/_2$	2.661	Pt−H = 1.544	2456
	bridge	$^{23}/_2$	2.607	Pt−H = 1.753	
	hcp	$^{23}/_2$	2.489	Pt−H = 1.863	
	fcc	$^{23}/_2$	2.618	Pt−H = 1.863	1317
$Pt_{9.10.9}$−O	top	9	2.015	Pt−O = 1.872	
	bridge	8	2.729	Pt−O = 1.990	
	hcp	8	2.946	Pt−O = 2.040 (2×)	531
				Pt−O = 2.151 (1×)	
	fcc	8	3.284	Pt−O = 2.005 (2×)	510
				Pt−O = 2.185 (1×)	

[a] For the most stable sites the frequency of the vibration mode perpendicular to the surface are given. All values for the oxygen adsorption are taken from ref 26.

TABLE 3: Ground Spin States, Adsorption Energies, and Bond Distances for Hydrogen Adsorption on Two Single-Layer Clusters ($Pt_{10}Ni_4$ and $Pt_{11}Ni_3$) and on the $Pt_{10.10.6}Ni_{4.3.2}$ Cluster, Which Gives the Best Representation of the Pt/Ni(111) Alloy Surface[a]

system		spin state	E (eV)	R (Å)	ω (cm^{-1})
$Pt_{10}Ni_4$−H	μ_1-Ni	$^7/_2$	1.643	Ni−H = 1.405	
	μ_1-Pt	$^7/_2$	3.244	Pt−H = 1.497	
	μ_2-PtNi	$^7/_2$	2.537	Pt/Ni−H = 1.677	
	μ_2-Pt_2	$^7/_2$	3.082	Pt−H = 1.740	
	fcc-Pt_2Ni	$^7/_2$	2.889	Pt/Ni−H = 1.801	
	fcc-Pt_3	$^9/_2$	2.773	Pt−H = 1.854	
		$^7/_2$	2.761	Pt−H = 1.859	
$Pt_{11}Ni_3$−H	μ_1-Ni	$^{11}/_2$	1.717	Ni−H = 1.400	
	μ_1-Pt	$^{11}/_2$	3.248	Pt−H = 1.500	
	μ_2-PtNi	$^9/_2$	2.540	Pt/Ni−H = 1.675	
	μ_2-Pt_2	$^9/_2$	3.326	Pt−H = 1.737	
	fcc-Pt_2Ni	$^{11}/_2$	2.885	Pt/Ni−H = 1.808	
	fcc-Pt_3	$^{11}/_2$	3.342	Pt−H = 1.859	
$Pt_{10.10.6}Ni_{4.3.2}$−H	μ_1-Ni	$^{21}/_2$	1.782	Ni−H = 1.439	1917
	μ_1-Pt	$^{21}/_2$	2.673	Pt−H = 1.556	2319
	μ_2-PtNi	$^{21}/_2$	2.598	Pt/Ni−H = 1.708	1450
	μ_2-Pt_2	$^{21}/_2$	2.411	Pt−H = 1.740	1337
	μ_2-Pt_2−B	$^{21}/_2$	2.483	Pt−H = 1.759	1522
	fcc-Pt_2Ni	$^{21}/_2$	2.551	Pt/Ni−H = 1.831	1750
	hcp-Pt_2Ni	$^{21}/_2$	2.356	Pt/Ni−H = 1.823	1205
	fcc-Pt_3	$^{19}/_2$	2.198	Pt−H = 1.832	1296
	hcp-Pt_3	$^{21}/_2$	2.269	Pt−H = 1.836	1158

[a] The vibrational frequencies obtained for this cluster are also listed.

4.2. Adsorption of Hydrogen. Because we want to obtain energies for all nine types of surface sites, independent of whether they are minima, we first minimized the energies consistent with the symmetry of this site (perpendicular to the surface for μ_1, in the plane perpendicular to the surface for μ_2 but starting with two equal bond distances, and no constraint for μ_3 but starting with three equal bond distances) and optimized the adsorbate−surface distances to minimize the energy. For most of the adsorption sites it turned out that the previously described constraints always allowed hydrogen to move to its most stable position. Thus, for all adsorption sites only the distance perpendicular to the surface was optimized. Because our examinations on the relaxation of both the Pt(111) surface and the Pt/Ni(111) alloy surface (see section 3.1) showed only 0.01 Å changes in the surface−subsurface bond distances upon optimization, we kept the distances between the atoms of the surface cluster fixed at the corresponding calculated bulk values (Pt(111), 2.775 Å; Pt/Ni(111), 2.755 Å).

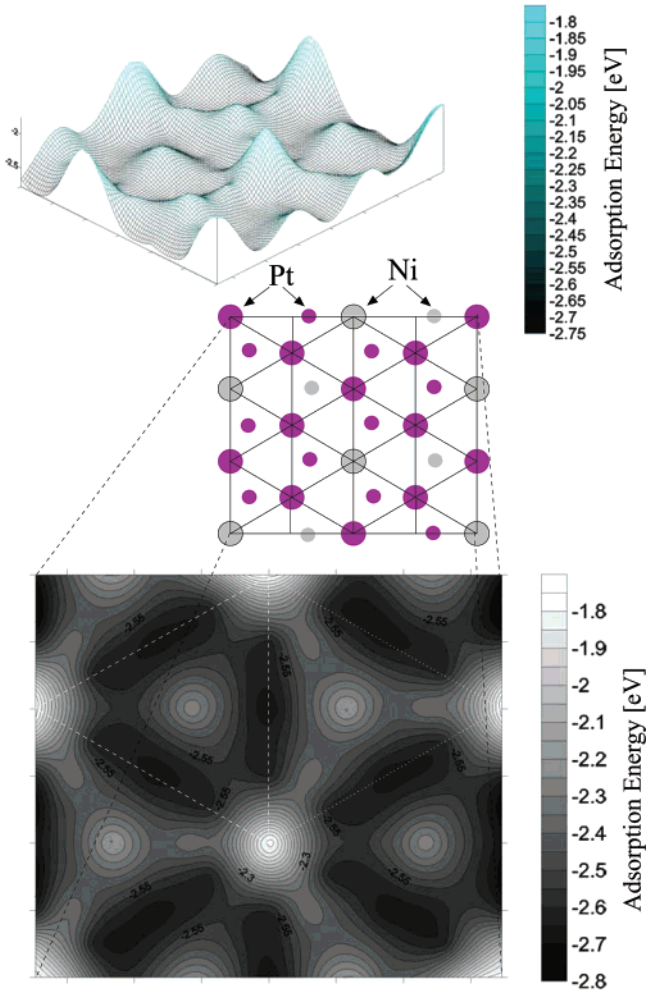

Figure 9. The upper surface plot and the lower contour plot show a global view of the adsorption energies for hydrogen on Pt/Ni(111) after a mininum curvature fit of the binding energies at all calculated sites. Both plots map the surface area shown in the central figure (small circles are second-layer atoms), where dark areas denote strong bonding. In addition, the dashed and dotted triangles in the contour plot define both different types of Ni-Δs (see section 4.4), with Ni-Δ/hcp on the left and Ni-Δ/fcc on the right.

On both single-layer clusters ($Pt_{10}Ni_4$ and $Pt_{11}Ni_3$) the ground spin states, adsorption energies, and bond distances were calculated at all six different surface sites: two on-top sites (μ_1-Pt and μ_1-Ni), two bridge sites (μ_2-Pt_2 and μ_2-PtNi), and also two 3-fold sites.

Afterward, the same procedure was applied to the $Pt_{10.10.6}$-$Ni_{4.3.2}$ cluster, which is assumed to represent well the properties of the 2D-periodic surface. In addition to the quantities examined for the one-layer systems, we also calculated the frequencies of the hydrogen vibrational modes perpendicular to the surface on the larger system. However, as discussed above, the multilayer cluster requires a third bridge site and two additional 3-fold sites to be considered, leading to nine possible surface positions (see Figure 8). All results on the hydrogen adsorption on the Pt/Ni(111) surface are given in Table 3. In addition, the data on pure Pt(111) are in Table 2. Moreover, all adsorption energies for the alloy surface were combined in a surface and a contour plot (see Figure 9).

4.2.1. H/Pt(111). For atomic hydrogen on pure Pt(111) our calculations led to similar adsorption energies at all four surface sites: 2.66 eV for on-top, 2.61 eV for bridge, 2.62 eV fcc-μ_3, and 2.49 eV for hcp-μ_3. We should point out here that these differences are comparable to the differences in zero point

TABLE 4: Ground Spin States, Adsorption Energies, and Bond Distances for Oxygen Adsorption on Two Single-Layer Clusters ($Pt_{10}Ni_4$ and $Pt_{11}Ni_3$) and on the $Pt_{10.10.6}Ni_{4.3.2}$ Cluster, Which Gives the Best Representation of the Pt/Ni(111) Alloy Surface[a]

system		spin state	E (eV)	R (Å)	ω (cm^{-1})	Q(O) (e)
$Pt_{10}Ni_4$−O	μ_1-Ni	6	1.608	Ni−O = 1.818		
	μ_1-Pt	5	2.222	Pt−O = 1.824		
	μ_2-PtNi	5	3.070	Pt−O = 1.916		
				Ni−O = 1.895		
	μ_2-Pt_2	4	3.192	Pt−O = 1.940		
	fcc-Pt_2Ni	4	3.889	Pt−O = 1.965		
				Ni−O = 1.936		
	fcc-Pt_3	3	3.577	Pt−O = 2.009 (2×)		
				Pt−O = 1.905 (1×)		
		4	3.570	Pt−O = 2.014 (2×)		
				Pt−O = 1.897 (1×)		
$Pt_{11}Ni_3$−O	μ_1-Ni	7	1.600	Ni−O = 1.811		
	μ_1-Pt	6	2.220	Pt−O = 1.822		
	μ_2-PtNi	6	3.010	Pt−O = 1.911		
				Ni−O = 1.901		
	μ_2-Pt_2	5	3.471	Pt−O = 1.942		
	fcc-Pt_2Ni	5	4.035	Pt−O = 1.956		
				Ni−O = 1.969		
	fcc-Pt_3	5	3.867	Pt−O = 1.962 (2×)		
				Pt−O = 2.051 (1×)		
$Pt_{10.10.6}Ni_{4.3.2}$−O	μ_1-Ni	11	1.639	Ni−O = 1.722	970	−0.34
	μ_1-Pt	11	1.834	Pt−O = 1.886	746	−0.42
	μ_2-PtNi	10	2.976	Pt−O = 1.978	649	−0.50
				Ni−O = 1.885		
	μ_2-Pt_2	10	2.456	Pt−O = 1.971	970	−0.52
	μ_2-Pt_2−B	10	3.270	Pt−O = 2.014	902	−0.53
	fcc-Pt_2Ni	10	3.501	Pt−O = 2.025	910	−0.56
				Ni−O = 2.016		
	hcp-Pt_2Ni	10	3.413	Pt−O = 2.033	967	−0.54
				Ni−O = 1.965		
	fcc-Pt_3	10	2.327	Pt−O = 2.117 (2×)	866	−0.53
				Pt−O = 1.941 (1×)		
	hcp-Pt_3	10	3.302	Pt−O = 2.152 (1×)	707	−0.53
				Pt−O = 2.055 (2×)		

[a] The vibrational frequencies and charge transfer to the oxygen obtained for this cluster are also listed.

energy (ZPE) for the different modes, which favor fcc-μ_3 over on-top by ≈0.14 eV. Thus, it is likely that experimental studies of H on Pt at low temperature would lead to fcc-μ_3 rather than on-top. In either case the barrier for H migration is low. These results (fcc-μ_3 site) are in good agreement with experimental observations (EELS)[34,35] and infrared reflection adsorption spectroscopy,[36] which find vibrational frequencies of 1230−1254 cm^{-1}, and with other theoretical calculations (periodic DFT at the LDA level including scalar-relativistic and spin−orbit effects),[37,38] which find 2263 cm^{-1} for the on-top and 1199 cm^{-1} for the fcc-μ_3 site. Moreover, the Pt−H bond length increases with respect to the number of adjacent Pt atoms (1-fold site, 1.544 Å; 2-fold site, 1.753 Å; both 3-fold sites, 1.863 Å). Because hydrogen has only one electron that should spin pair with an unpaired surface orbital to form a covalent bond, we expected the ground spin state of the Pt(111) surface cluster (S = 11) to reduce by $^1/_2$. This is exactly what we found in the calculations.

The large difference in bond energy between the fcc-μ_3 and hcp-μ_3 sites can be rationalized in terms of the interstitial electron model (IEM). In this model the delocalized sp electrons tend to localize in interstitial tetrahedral positions, putting them just below the hcp-μ_3 site. Thus, bonding H at this site should disrupt some of this bonding.

4.2.2. H/Pt_3Ni(111). Alloying of the Pt(111) surface with Ni dramatically changes the adsorption behavior of hydrogen. To discuss these effects, we will focus on the $Pt_{10.10.6}Ni_{4.3.2}$ alloy cluster, which was found to be the best surface model.

We find that the Pt on-top site leads to the same bond strength as previously (2.67 eV compared to 2.66 eV), consistent with a localized model of bonding. In addition, the vibrational frequency decreases by about 5% and the Pt−H bond distance increases by less than 1%, indicating that alloying the Pt(111) with Ni does not change the bonding at the Pt top site. However, the Ni on-top site leads to a bond strength weaker by 0.89 eV! This is no doubt because the bonding at this site is dominated by d character, which for Ni is much too small to make a good bond to H.[39] Both μ_2-Pt_2 bridge sites lead to weaker bonds (2.41 and 2.48 eV) than the 2.60 eV for pure Pt, but the μ_2-PtNi bridge site also leads to 2.60 eV.

Among the four μ_3 sites, the most stable is fcc-Pt_2Ni with 2.55 eV. Comparing μ_3-Pt_2Ni sites, hcp is 0.19 eV higher, similar to the difference of 0.13 eV for pure Pt. However, for the μ_3-Pt_3 sites, the fcc position is disfavored over hcp by 0.07 eV, and the total bond strength of 2.20 eV is quite weak compared to fcc-Pt_2Ni. Clearly this site bonds differently, because the ground spin decreases by $^3/_2$ rather than $^1/_2$, as found for all other cases. This implies that the bonding at this site involves what would have been an excited S = 10 state of the original cluster. The difference in bonding is reflected in the vibrational frequencies, which leads to 1750 cm^{-1} for the favorable fcc-Pt_2Ni site, but to 1158−1296 cm^{-1} for the other three sites. This can be compared to experimentally measured vibrational frequency of 1230−1254 cm^{-1} for the fcc-μ_3 site on pure Pt.[34−36]

The result of the range of adsorption energies from 1.78 eV (μ_1-Ni) to 2.67 eV (μ_1-Pt) is a much more rugged energy surface than for pure Pt, leading to a significantly more localized hydrogen on the alloy surface. This is shown in Figure 9. We find that starting with the favorable μ_1-Pt on-top site, the barrier

for moving to another μ_1-Pt site via the μ_2-Pt_2−B bridge with the subsurface Ni is 0.19 eV, whereas the barrier for the pathway involving the μ_2-Pt_2 bridge is 0.28 eV. Thus, the favorable migration of H is between the triangle of three Pt sites that share a subsurface Ni. From each of these three sites it is uphill only 0.06 eV for the H to go to the two adjacent μ_2-PtNi bridge sites. From there it is a total of 0.12 eV to go to the adjacent hcp-Pt_2Ni sites (but not the adjacent fcc-Pt_2Ni site). Thus, the lower energy pathway is for on-top H to go to a μ_2-PtNi bridge, then to hcp-Pt_2Ni, then to the other μ_2-PtNi bridge, and finally to the adjacent μ_1-Pt site, with a total barrier of only 0.12 eV. However, the direct hop via the μ_2-Pt_2−B bridge (with Ni subsurface) might have more contributions from tunneling.

Migration from one of the on-top triangles (see Figure 9) to an adjacent one involves a barrier of 0.28 eV. Thus, even though the landscape is more rugged on the Pt/Ni alloy, the H can delocalize over the surface quite readily. Ignoring ZPE, the barrier for migration increases from 0.05 to 0.28 eV, but at operation temperatures of fuel cells this should still be rapid.

Finally, we note that the ground spin states are $^{21}/_2$ for nearly all clusters with hydrogen adsorbed at different sites. Because the ground state spin of the pure $Pt_{10.10.6}Ni_{4.3.2}$ system is $S = 11$, this means that bonding the H causes the spin to decrease by $\Delta S = {}^1/_2$. This is exactly the same as observed on Pt(111) and is the result expected for a covalent bond to the surface. The only exception arises for adsorption at the fcc-Pt_3 site, which causes a decrease of the ground spin state by $\Delta S = {}^3/_2$. Because this site also shows deviation from the other 3-fold site during oxygen adsorption, further discussions about this will be deferred to section 4.4.

4.3. Adsorption of Oxygen. The adsorption energies and bond distances for oxygen on the alloy surface were obtained at the same nine positions as discussed above for hydrogen. The previously obtained results for oxygen chemisorption on pure Pt(111)[26] led to adsorption energies as follows for the four surface sites: 3.28 eV for fcc-μ_3, 2.95 eV for hcp-μ_3, 2.73 eV for bridge, and 2.02 eV for on-top.

On pure Pt oxygen binds most strongly at the fcc site with an adsorption energy of 3.28 eV, which can be compared to experimental values that range between 3.21 and 3.43 eV.[40] Here we find two short Pt−O bonds at 2.01 Å (indicating two covalent bonds), with the distance to the third Pt atom longer by 0.18 Å (suggesting a donor−acceptor bond). This is roughly the (≈0.2 Å) difference in bond distance generally observed for a bond order change of 1 (thus ethane has C−C = 1.54 Å and ethene 1.34 Å).[41] The experimentally measured bond length is 2.01 ± 0.05 Å,[42] in very good agreement with our result. These data and those for the other adsorption sites are summarized in Table 2.

Because oxygen has two unpaired electrons for the pure Pt surface we found that oxygen chemisorption changes the ground spin state of the cluster by $\Delta S = 1$ for the μ_2 and μ_3 sites. The same behavior was observed for the alloy. On pure Pt the on-top bond spin pairs just the σ-spin of O to a σ-spin of a surface Pt, leaving an unpaired π-spin on the oxygen. The result is no net change in spin and a short bond indicating a bond order of ≈1.5. Exactly the same result was observed for both on-top sites of the alloy.

In discussing the oxygen adsorption on the Pt_3Ni(111) alloy surface we also will only analyze the results for the $Pt_{10.10.6}$-$Ni_{4.3.2}$ alloy cluster. More complete results on the oxygen adsorption on the alloy surface are summarized in Table 4.

4.3.1. Binding at μ_3 Sites. It turned out that on the alloy oxygen is most strongly bound at the fcc-Pt_2Ni site with 3.50 eV. This is much stronger than the 3.28 eV for pure Pt. Moreover, the hcp-Pt_2Ni site is only 0.09 eV less, whereas for pure Pt it was 0.33 eV worse. On the other hand, the fcc-Pt_3 site is quite unfavorable compared to the fcc-Pt_2Ni site (by 1.17 eV), whereas the hcp-Pt_3 site is only 0.20 eV above the ground state. Clearly, there is something bad about the fcc-Pt_3 site. However, the net spin of the system for this site and the others is $S = 10$ (cluster without adsorbate: $S = 11$), indicating that two unpaired spins from the bare cluster are covalently coupled to the O atom. In addition, the bond energies and vibrational frequencies seem similar (866−967 cm^{-1}) for all four μ_3 sites of the alloy, but much larger than for pure Pt (510 and 531 cm^{-1}).

Although there is a great deal of experimental data for oxygen chemisorption on Pt(111), we find no site-selective values available for the Pt_3Ni(111) alloy surface.

The weaker bond energy at the μ_3-Pt_3 sites can be explained by the distribution of the net spin density at each site. Analyzing the Mulliken charges, we find a net spin of 1.1−1.3 at each surface Ni, and less than 0.5 on the Pt atoms. This should be compared to the pure Pt surface, where the average net spin of the first-layer atoms is about 0.7. This reduction in the net spin makes binding to three Pt atoms much less favorable on the alloy than on pure Pt(111). This may also explain why binding at the fcc (no atom in the second layer) site is weaker than at the hcp site (additional Pt atom in the second layer beneath the 3-fold site). Because binding to the surface oxygen needs to spin pair its two unpaired electrons and because the μ_3-Pt_3 site is deficient in unpaired spins, it may be that the fourth Pt atom with its additional unpaired spin helps making hcp more favorable.

For fcc-Pt_2Ni the bond distances to the two Pt are 2.03 Å, quite similar to the pure Pt surface (2.01 Å), indicating covalent bonds. Hence the O−Ni bond of 2.02 Å is much longer than the bond distance for an O−Ni covalent bond (1.89 Å, the bond distance for the μ_2-PtNi bridge site). Thus, the increase in bond distance for the donor−acceptor bond in the fcc-Pt_2Ni site is just 0.13 Å longer than a covalent bond. This indicates somewhat stronger bonding, which may result from the greater ionic character (Ni is much more electropositive than Pt or O), perhaps explaining the stronger bond. The remaining 3-fold sites all show behavior in the bond distances similar to that observed for oxygen on Pt(111), namely one elongated and two short bonds.

4.3.2. Binding at μ_2 Sites. The best bridge site is the μ_2-Pt_2−B with a Ni beneath the bridge. This has a bond energy of 3.27 eV, which is 0.54 eV stronger than the bridge site for pure Pt. The Pt−O bonds (2.01 Å) are normal (they were 1.99 Å on the pure Pt(111) surface), indicating that the site makes good covalent bonds despite the low spins on the surface Pt. We suspect that this must be due to the spins available on the subsurface Ni. The vibrational frequency of 902 cm^{-1} seems low compared to the μ_3-Pt_2Ni site with 910 cm^{-1}.

The μ_2-PtNi bridge site has a bond energy of 2.98 eV, leading to a Pt−O bond length of 1.98 Å and a Ni−O bond length of 1.89 Å, which we take as the length of covalent bonds. Here the vibrational frequency of 649 cm^{-1} seems quite low.

The μ_2-Pt_2 bridge site with a subsurface Pt is much weaker with a bond energy of only 2.46 eV. As with the fcc-Pt_3 site, it appears that the μ_2-Pt_2−B position is poor because of a lack of unpaired d orbitals available to make covalent bonds. On the other hand, the Pt−O bonds are short (1.97 Å) and the vibrational frequencies are high (970 cm^{-1}).

4.3.3. Binding at μ_1 sites. As for pure Pt, the on-top binding on the alloy does not change the ground spin state of the system. This supports the model that the σ-bond is between a singly occupied O p$-\sigma$ orbital and a singly occupied Pt d$-\sigma$ orbital. This leaves behind an O p$-\pi$ orbital, which can contribute to a half-order π-bond to the surface, resulting in no net change in the spin and a bond length 0.14 Å shorter than for the μ_3 site (the difference was 0.13 Å on pure Pt(111)). However, the vibrational frequency of 746 cm^{-1} seems unreasonably low for an on-top site. The bond energy for the alloy is 1.83 eV, which is 0.19 eV weaker than for pure Pt. These results indicate that binding to the Pt on-top site is not much affected by the alloying.

Binding of O to the Ni-top site is weaker by 0.20 eV, and the bond distance is 0.16 Å shorter than the single bond. The spin change upon bonding is zero. These results all indicate a bond similar in character to the Pt on-top site.

4.3.4. Comparison to Single-Layer Calculations. Comparing the adsorption energies for the alloys obtained using the single-layer clusters with those of the three-layer system shows an agreement for the μ_1-Ni, μ_2-PtNi, and μ_2-Pt_2 (μ_2-Pt_2−B bridge for $Pt_{10.10.6}Ni_{4.3.2}$) sites. All other sites (μ_1-Pt, and all μ_3 positions) have adsorption energies higher by ≈0.4 eV for the single-layer clusters. Similar relations between the one-layer and the three-layer systems were observed for the oxygen adsorption on pure Pt(111).[26]

The bond distances are shorter for most adsorption sites on the one-layer clusters, as expected from the stronger bonds.

These results show that even for the alloy surface one-layer clusters give reasonable results on the relative binding energies and bond distances for the strongest adsorption sites. Clearly, there will be problems in distinguishing hcp and fcc sites because there are no subsurface atoms. Thus, the one-layer clusters may be useful for mapping out the energy surfaces of catalytic processes.

4.4. Comparison. In this section we combine all calculated adsorption energies at the various surface positions for hydrogen and oxygen. This overall picture of the behavior of the alloy surface during both adsorption processes is shown in Figure 9 for hydrogen and Figure 10 for oxygen. Both figures and especially the contour plots, which are shown in the lower part of the figures, are the basis for the following discussion.

4.4.1. H-Migration. As mentioned in section 4.2, hydrogen is most strongly bound on-top of a Pt atom and weakest on-top of a Ni atom. Because every Ni is surrounded by six Pt atoms, each triangle connecting the three closest Ni atoms has three Pt inside (hereafter Ni-Δ); a hydrogen atom that adsorbs on the Pt/Ni(111) surface will mainly be localized inside of a Ni-Δ. However, there exist two types of Ni-Δ's. One, denoted as Ni-Δ/fcc has three Pt atoms inside, where no atom is in the second layer beneath this 3-fold side (fcc-Pt_3). The other type, denoted as Ni-Δ/hcp, has a hcp-Pt_3 site, which means there is an atom in the second layer below. First, we will discuss the preferred hydrogen position inside Ni-Δ/hcp. Because this Ni-Δ/hcp has a hcp-Pt_3 site in the center, all adjacent 3-fold sites are fcc-Pt_2-Ni. Therefore, the barrier to move hydrogen from one most stable site (μ_1-Pt) to another is determined by the energy difference (fcc-Pt_2Ni) − (μ_1-Pt) (0.12 eV). The low-energy barrier causes a highly mobile hydrogen around the hcp-Pt_3 site, which is indicated by the three dark areas on the upper left part in the contour plot of Figure 9. For the Ni-Δ/fcc the behavior is different. Inside this Ni-Δ the barrier to move hydrogen between two μ_1-Pt sites is limited by μ_2-Pt_2; thus the barrier is 0.26 eV. Because each Ni-Δ/fcc is only next to Ni-Δ/hcp, each Pt atom is part of both types of Ni-Δs. Therefore, to transfer from one μ_1-Pt site to another, the hydrogen atom must move between different Ni-Δs. However, after arriving at a Ni-Δ/hcp, the energy barrier to stay inside this Ni-Δ is lower by 0.14 eV than moving to an adjacent Ni-Δ. This leads to the following picture for the diffusion of hydrogen adsorbed on the Pt/Ni(111) surface:

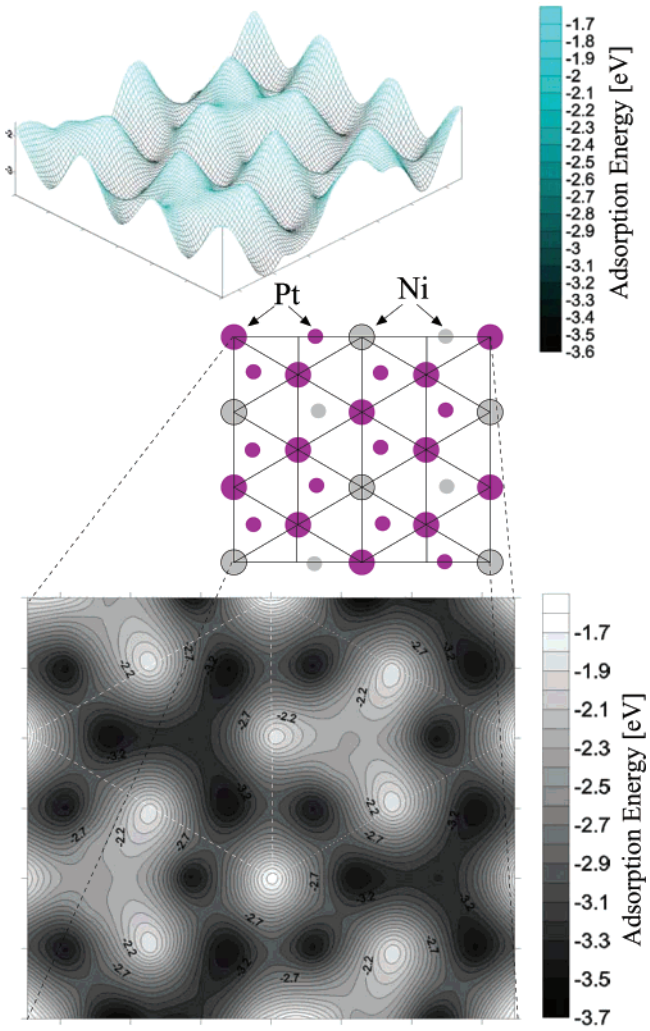

Figure 10. Upper surface plot and the lower contour plot showing a global view of the adsorption energies for oxygen on Pt/Ni(111) after a mininum curvature fit of the binding energies at all calculated sites. Both plots map the surface area shown in the central figure (small circles are second-layer atoms), where dark areas denote strong bonding. In addition, the dashed and dotted triangles in the contour plot define both different types of Ni-Δs (see section 4.4), with Ni-Δ/hcp on the left and Ni-Δ/fcc on the right.

- Low kinetic energy (<0.26 eV) means that hydrogen is mostly located around hcp-Pt_3 sites.
- Kinetic energies greater than 0.26 eV mean that, depending on the kinetic energy, hydrogen has a higher surface mobility and is mainly located around hcp-Pt_3 and fcc-Pt_3 sites.

4.4.2. O-Migration. The behavior for adsorbed oxygen is different. Because oxygen has a strong influence on the electronic structure of the surface, the mobility and preferred surface areas are different from hydrogen. For pure Pt(111), O at its most stable fcc site would be favorable to hop to an adjacent hcp site (with an energy 0.33 eV higher) through the bridge site, leading to a barrier for migration of 0.55 eV (as discussed above we have not included ZPE effects here, which would be smaller for O motion). This motion can lead to migration over all fcc sites on the surface.

On the alloy oxygen was found to bind most strongly at the fcc-Pt_2Ni site. Applying the same picture of Ni-Δs that we used for the hydrogen adsorption, all fcc-Pt_2Ni sites belong to Ni-Δ/hcp. According to the contour plot shown in Figure 10 there are two possible pathways for movement between the fcc-Pt_2-Ni sites. If both the initial and final fcc-P_2Ni sites belong to the same Ni-Δ/hcp, oxygen may use the following pathway: (fcc-Pt_2Ni)−(μ_2-Pt_2−B)−(hcp-Pt_3)−(μ_2-Pt_2−B)−(fcc-Pt_2Ni). The energy barrier for this pathway is 0.23 eV ((fcc-Pt_2Ni) − (μ_1-Pt_2−B)). The other pathway is between two fcc-Pt_2Ni sites of different Ni-Δs. Because Ni-Δs of the same type are not next to each other, the second pathway includes intermediate positions of both types of Ni-Δs and can be seen as a circle around a Ni atom: (fcc-Pt_2Ni)−(μ_2-PtNi)−(hcp-Pt_2Ni)−(μ_2-PtNi)−(fcc-Pt_2Ni). For this pathway the energy barrier is 0.52 eV ((fcc-Pt_2Ni) − (μ_2-PtNi)). Because the adsorption at fcc-Pt_3 is much less favorable than all other 3-fold and all 2-fold sites, there is less probability for an oxygen atom to be located near to the center of a second-type Ni-Δ (center position is fcc-Pt_3). Finally, this leads to the following for oxygen preferred surface areas:

•Kinetic energies less than 0.52 eV cause oxygen to be localized mainly inside one type of Ni-Δs and there moving between the possible 3-fold sites (fcc-Pt_2Ni and hcp-Pt_3). Thus, there is facile motion of the O through a "star" symbol of sites. But the barrier to go from one "star" symbol to another requires going through a μ_2-PtNi bridge and hence a barrier of 0.52 eV.

•With higher kinetic energies (>0.52 eV) the probability to move between fcc-Pt_2Ni sites of different Ni-Δs (over next fcc-Pt_2Ni position) increases. Thus, oxygen is able to move between all fcc-Pt_2Ni sites of the surface and is not restricted to a certain Ni-Δ. Therefore, the picture of oxygen moving in channels on the surface (see dark areas in contour plot of Figure 10) arises.

5. Summary

The main aim of this paper was to determine the optimal composition of the Pt/Ni alloy in the bulk and on the surface, and then to study the electronic structure of the Pt/Ni(111) alloy surface by calculating the adsorption of atomic hydrogen and oxygen on all possible surface sites. To obtain the optimal composition, we considered clusters with a variety of sizes and shapes up to 44 atoms and up to three layers. From systematic changes in the ratio and distribution of Pt and Ni atoms, we found that the alloy surface prefers the same structure as the Pt_3Ni fcc-like crystal bulk phase. This leads to a (111) surface in which every Ni atom is surrounded by six Pt atoms. In addition, this leads to a 3:1 ratio between Pt and Ni on the surface. For the adsorption studies we used the calculated bulk and surface Pt/Ni composition with the cluster found to best representation of the (111)-surface ($Pt_{10.10.6}Ni_{4.3.2}$).

For both hydrogen and oxygen, chemisorption on the alloy cluster and on the pure Pt cluster showed exactly the same behavior of the ground spin-state changes. This validates our basic model of covalent bonding of H and O to the surface d orbitals. However, the Ni atoms in the alloy system drastically influence the electronic configuration of the system and therefore the binding of oxygen and hydrogen atoms. On the $Pt_3Ni(111)$ alloy surface the oxygen is more strongly bound by 0.22 eV than on Pt(111), but the adsorption energies range from 1.64 eV (μ_1-Ni) to 3.50 eV (fcc-Pt_2Ni) (pure Pt: 2.02−3.28 eV). Thus, in one sense oxygen is much more localized on Pt/Ni than on pure Pt. However, there is a smaller barrier (0.26 eV) for O to move between a triangle of adjacent fcc-Pt_2Ni sites whereas the long-range migration barrier is about the same as for pure Pt (0.56 eV), but the motion of oxygen is through surface channels.

For hydrogen the adsorption energies at the different surface sites vary much more on Pt/Ni(111) (1.78−2.67 eV) than on pure Pt(111) (2.49−2.66 eV). The net barrier for long-range diffusion of H on the surface (0.26 eV) is 5 times as high as for pure Pt, but there is still a low barrier (0.12 eV) for the H to hop between three adjacent Pt on-top sites. Comparing the preferred surface areas for hydrogen and oxygen, we see both overlap and differences.

It turned out that the oxygen atom binds more strongly on the Pt/Ni alloy than on pure platinum and that the positions of both elements (H and O) are more localized on the alloy surface. Both aspects might play an important role in enhancing the ORR and therefore the reaction rate of the catalytic cathode process. Thus the stronger bond of the oxygen atom to the surface may reduce the barrier for dissociating O_2 on the surface.

Acknowledgment. T.J. gratefully acknowledges support by the German academic exchange service (DAAD). This work was also supported by General Motors (Gerald Voecks). The computation facilities of the MSC have been supported by grants from ARO-DURIP, ONR-DURIP, NSF (MRI, CHE), and IBM-SUR. In addition, the MSC is supported by grants from DoE ASCI, ARO-DARPA, ONR-MURI, NIH, ONR, Chevron-Texaco, Seiko-Epson, Beckman Institute, and Asahi Kasei.

References and Notes

(1) Gottesfeld, S.; Zawodzinski, T. A. In *Polymer electrolyte fuel cells*; Alkire, R. C., Gerischer, H., Kolb, D. M., Tobias, C. W., Eds.; Advances in Electrochemical Science and Engineering, Vol. 5; Wiley-VCH: Weinheim, 1997.

(2) Wilson, M. S.; Valerio, J. A.; Gottesfeld, S. *Electrochim. Acta* **1995**, *40*, 355.

(3) Beard, B. C.; Ross, P. N. *J. Electrochem. Soc.* **1990**, *137*, 3368.

(4) Glass, J. T.; Cahen, G. L.; Stoner, G. E.; Taylor, F. J. *J. Electrochem. Soc.* **1987**, *134*, 58.

(5) Min, M.; Cho, J.; Cho, K.; Kim, H. *Electrochim. Acta* **2000**, *45*, 4211.

(6) Tamizhmani, G.; Capuano, G. A. *J. Electrochem. Soc.* **1994**, *141*, 968.

(7) Paulus, U. A.; Wokaun, A.; Scherer, G. G.; Schmidt, T. J.; Stamenković, V.; Marković, N. M.; Ross, P. N. *Electrochim. Acta* **2002**, *47*, 3787.

(8) Stamenković, V.; Schmidt, T. J.; Ross, P. N.; Marković, N. M. *J. Phys. Chem. B* **2002**, *106*, 11970.

(9) Vasiliev, M. A. *J. Phys. D* **1997**, *30*, 3037.

(10) Lundberg, M. *Phys. Rev. B* **1987**, *36* (9), 4692.

(11) Hansen M.; Anderko, K. *Constitution of Binary Alloys*; McGraw-Hill: New York, 1958.

(12) Bardi, U.; Beard, B. C.; Ross, P. N. *J. Catal.* **1990**, *124* (1), 22.

(13) Gauthier, Y.; Joly, Y.; Baudoing, R.; Rundgren, J. *Phys. Rev. B* **1985**, *31*, 6216.

(14) Becke, A. D. *J. Chem. Phys.* **1993**, *98* (7), 5648.

(15) Lee, C.; Yang, W.; Parr, R. G. *Phys. Rev. B* **1988**, *37*, 785.

(16) Xu, X.; Goddard, W. A., III. *Proc. Natl. Acad. Sci. USA* **2004**, *101*, 2673.

(17) Slater, J. C. *The Self-Consistent Field for Molecules and Solids*; Quantum Theory of Molecules and Solids, Vol. 4; McGraw-Hill: New York, 1974.

(18) Becke, A. D. *Phys. Rev. A* **1988**, *38*, 3098.

(19) Vosko, S. H.; Wilk, L.; Nusair, M. *Can. J. Phys.* **1980**, *58*, 1200.

(20) Jaguar 4.2, Schrödinger Inc.; Portland, Oregon, 2000.

(21) Hay, P. J.; Wadt, W. R. *J. Phys. Chem.* **1985**, *82*, 299.

(22) Goddard, W. A., III. *Phys. Rev.* **1968**, *174*, 659.

(23) Kahn, L. R.; Goddard, W. A., III. *J. Chem. Phys.* **1972**, *56*, 2685.

(24) Melius, C. F.; Olafson, B. D.; Goddard, W. A., III. *Chem. Phys. Lett.* **1974**, *28*, 457.

(25) Melius, C. F.; Goddard, W. A., III. *Phys. Rev. A* **1974**, *10*, 1528.

(26) Jacob, T.; Muller, R. P.; Goddard, W. A., III. *J. Phys. Chem. B* **2003**, *107* (35), 9465.

(27) Schultz, P. A. Unpublished. A description of the method is in: Feibelman, P. J. *Phys. Rev. B* **1987**, *35*, 2626.
(28) Perdew, J. P.; Burke, K.; Ernzerhof, M. *Phys. Rev. Lett.* **1996**, *77*, 3865.
(29) Hamann, D. R. *Phys. Rev. B* **1989**, *40*, 2980.
(30) Kittel, Ch. *Einführung in die Festkörperphysik*; R. Oldenbourg Verlag: München, 1991.
(31) Donohue, J. *The structures of the elements*; Wiley: New York, 1974.
(32) Kua, J.; Goddard, W. A., III. *J. Phys. Chem. B* **1998**, *102* (47), 9481, 9492.
(33) Jacob, T.; Goddard, W. A., III. *J. Am. Chem. Soc.*, submitted for publication.
(34) Baró A. M.; Ibach, H.; Bruchmann, H. D. *Surf. Sci.* **1979**, *88*, 384.
(35) Richter, L. J.; Ho, W. *Phys. Rev. B* **1987**, *36*, 9797.
(36) Reutt J. E.; Chabal, Y. J.; Christman, S. B. *J. Electron Spectrosc. Relat. Phenom.* **1987**, *44*, 325.
(37) Olson, R. A.; Kroes, G. J.; Baerends, E. J. *J. Chem. Phys.* **1999**, *111* (24), 11155.
(38) Papoian, G.; Nørskov, J. K.; Hoffmann, R. *J. Am. Chem. Soc.* **2000**, *122*, 4129.
(39) Upton, T. H.; Goddard, W. A., III. *CRC Crit. Rev. Solid State Mater. Sci.* **1981**, *10* (3), 261.
(40) Parker, D. H.; Bartram, M. E., Koel, B. E. *Surf. Sci.* **1989**, *17*, 489.
(41) Ramachandran, S.; Tsai, B.-L.; Blanco, M.; Chen, H.; Tang, Y.; Goddard, W. A., III. *J. Phys. Chem. A* **1997**, *101*, 83.
(42) Materer, N.; Starke, U.; Barbieri, A.; Döll, R.; Heinz, K.; van Hove, M. A.; Somorjai, G. A. *Surf. Sci.* **1995**, *325*, 207.